Proton Dynamics in Interacting Hydrogen Bonds in the Solid State: Proton Tunneling in the NHO Hydrogen Bonds of N,N′-Di(2-Hydroxy-1-Naphthylmethylene)-p-Phenylenediamine

Sadamu Takeda[1,*], Tamotsu Inabe[2], Claudia Benedict[3], Uwe Langer[3], and Hans-Heinrich Limbach[3]

[1] Department of Chemistry, Faculty of Engineering, Gunma University, Kiryu, Gunma 376 8515, Japan
and Institute for Molecular Science, Myodaiji, Okazaki 444 8585, Japan
[2] Division of Chemistry, Graduate School of Science, Hokkaido University, Sapporo 060 0810, Japan
[3] Institut für Organische Chemie, Freie Universität, Berlin, Fachbereich Chemie, Takustraße 3, D-14195 Berlin, Germany

Key Words: Hydrogen Bond / Molecular Interactions / Proton Transfer / Spectroscopy, Nuclear Magnetic Resonance / Tunneling

Combination of comprehensive investigations of the spin-lattice relaxation rate of proton and low temperature ^{15}N-CP/MAS NMR spectrum provides unique information of proton dynamics in two interacting NHO hydrogen bonds of solid N,N′-di(2-hydroxy-1-naphthylmethylene)-p-phenylenediamine (DNP). It was evidenced from the ^{1}H-NMR relaxation measurement that tunneling mechanism operates for the proton transfer in the hydrogen bonds. The tunneling phenomenon is closely related to the very small energy differences among the four tautomeric states accompanied with the proton transfer in the two NHO hydrogen bonds. The very small values of the energy difference, in spite of the chemically asymmetric NHO hydrogen bond, were revealed by the ^{15}N-CP/MAS NMR spectrum. This is a unique character of solid DNP. It was also suggested from the derived energy scheme of the four tautomers and activation energies of the proton transfer that an interaction exists between the two NHO hydrogen bonds linked by π-electronic molecular frame. This means that the information of one NHO hydrogen bond, i.e. OH-form or NH-form, propagates to the other hydrogen bond and the proton transfer in the first hydrogen bond induces the change of the potential function for the proton transfer in the second hydrogen bond.

1. Introduction

Salicylideneaniline derivatives have attracted considerable attention because of their thermochromic or photochromic properties [1]. The mechanism of these processes has been assigned to proton transfer processes in the NHO hydrogen bonds of these molecules [2]. As these bonds are part of an electronically quasi-conjugated network, proton transfer between oxygen and nitrogen induces a change of the electronic state i.e. to a color change.

Particularly interesting is the case of salicylideneaniline derivatives exhibiting two NHO proton transfer units which interact through the quasi-π-conjugated network. In these cases, proton transfer from oxygen to nitrogen atom in one hydrogen bond giving rise to a change of the local electronic structure can also change the potential for the proton motion in the second NHO-bond as depicted schematically in Fig. 1. Depending on a number of parameters such as molecular structure, crystal structure and temperature the proton transfer may occur either by ground state or vibrationally assisted tunneling through the barrier or may proceed over the barrier. Correlated double proton transfers in NHN hydrogen bonds have also been observed in a number of other dyes using liquid [3] and solid state [4, 5] NMR spectroscopy, where these processes are, however, not associated with color changes as the electronic properties of the various tautomers are very similar. The present solid state NMR study of the

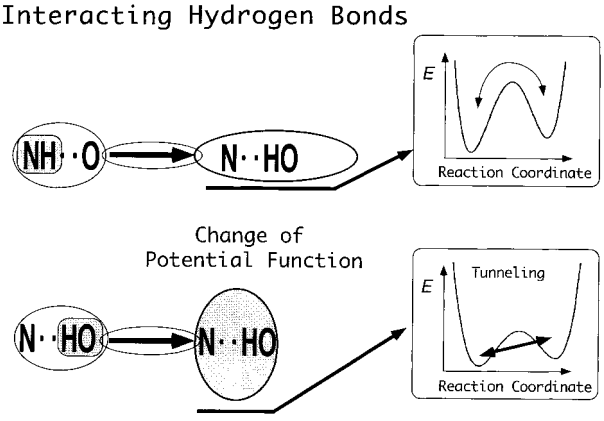

Fig. 1
Schematic view of interacting hydrogen bonds. Information of one hydrogen bond propagates to the other hydrogen bond

title compound N,N′-di(2-hydroxy-1-naphthylmethylene)-p-phenylenediamine (DNP, Fig. 2) exhibiting two interacting NHO-proton transfer units was, therefore, performed because of the following reasons. Firstly, such systems are interesting models for the study of the interacted tunneling and classical motion of two protons in different parts of a molecule. Secondly, the understanding of these systems may help to construct new materials exhibiting interesting electronic properties based on the proton motion.

As indicated in Fig. 2, the NHO hydrogen bonds of DNP are not linear but slightly bent, where the N···O distance is remarkably short, i.e. $R(\mathrm{N}\cdots\mathrm{O}) = 0.2537$ nm [6]. The difference Fourier map determined by X-ray dif-

*) Corresponding author (E-mail: stakeda@chem. gunma-u.ac.jp, Fax: (+81) 277 30 13 80)

  0005-9021/98/1010-1358 $ 17.50+.50/0

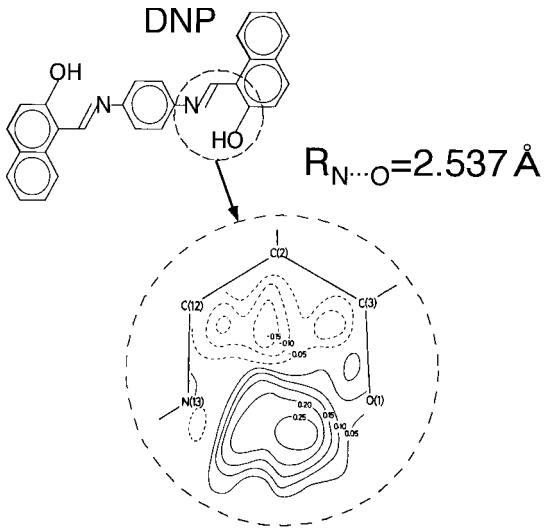

Fig. 2
Structure of DNP molecule. Insert is the difference synthesis of the electron distribution determined by X-ray diffraction experiment [6], showing the delocalization of the hydrogen atom in the hydrogen bond

fraction at room temperature indicates considerable delocalization of proton in the NHO hydrogen bonds and the proton transfer seems to occur in this crystal. Near-edge X-ray absorption fine structure (NEXAFS) spectroscopy at the N K- and O K-edges and X-ray photoelectron spectroscopy (XPS) in the N1s and O1s regions also indicated the existence of both OH and NH forms of the hydrogen bond [7]. Thus, the DNP crystal is a good candidate for investigating precisely the dynamics of the proton transfer and the possible interaction between the hydrogen bonds. The proton transfer dynamics was investigated by the measurements of relaxation rate of ^{1}H-NMR and ^{15}N-CP/MAS NMR techniques. Preliminary result of the ^{15}N-CP/MAS NMR has been published [8]. In this paper the precise discussions are presented from the combination of the relaxation rate of ^{1}H-NMR and the chemical shift of ^{15}N-CP/MAS NMR.

2. Experimental

2.1 Materials

The methods of preparation of the material and the crystal structure have been reported [6]. Doubly ^{15}N labeled DNP was prepared by condensation of $^{15}N_2$-p-phenylenediamine with 2-hydroxy-1-naphthylaldehyde [8].

2.2 ^{15}N-CP/MAS NMR Measurement at Very Low Temperatures

^{15}N-CP/MAS NMR spectrum of DNP was measured with different two spectrometers. In Berlin the ^{15}N-CP/MAS NMR measurements were performed between 130 K and 400 K at the resonance frequency of 9.12 MHz for ^{15}N [8].

The ^{15}N chemical shift at very low temperature was measured with Bruker DSX 400 spectrometer equipped with a low temperature CP/MAS NMR probe (Doty Penguin probe) at Institute for Molecular Science (IMS), Okazaki, Japan. Sample spinning rate was between 2.0 and 3.7 kHz and more than 2 kHz was achieved at 26 K. Driving and bearing gas was helium gas which was directly supplied from the liquid helium vessel to the CP/MAS probe with maintaining manually the pressure at ca. 0.3 bar. The temperature was controlled automatically. After the temperature became stable at the set point, time period of ca. 30 minutes was taken to establish the homogeneous temperature around the sample. This procedure avoided the artificial hysteresis of the chemical shift between the measurements in the direction of decreasing and increasing temperature. Fluctuation of the temperature was less than ±2 K for each set temperature. The thermometer of the Penguin probe was not calibrated by NMR method, since no appropriate reference material is known. As we discuss in the next section, the plot of all the data showed no apparent gap between the shift values measured with the two NMR probes. Other experimental conditions for Penguin probe are 40.55 MHz resonance frequency for ^{15}N, 15 μs π/2-pulse, 2 ms CP time, 1 (26 K) to 80 (306 K) scans on average and 8 to 300 s for repetition time. The chemical shift was measured from the solid $^{15}NH_4Cl$ (95% ^{15}N enriched). The chemical shift of $^{15}NH_4Cl$ is located at –341.2 ppm from liquid nitromethane [9]. For the experiment with low temperature CP/MAS probe, ^{15}N-glycine (–347.5 ppm from liquid nitromethane) was used as an internal reference.

2.3 ^{1}H-NMR Relaxation Measurement

The pulverized specimen was dried under vacuum and was sealed-off into glass ampul with helium gas of 20 mmHg for the heat exchange. The spin-lattice relaxation rate T_1^{-1} of proton was determined by π/2-train-τ-π/2 pulse sequence at resonance frequencies of 18 and 37 MHz. The temperature was kept constant within ±0.2 K for each set temperature and was measured by calibrated Chromel-p-constantane and Au(Fe)-chromel thermocouples.

3. Experimental Results

3.1 ^{15}N-CP/MAS NMR

Isotropic shift of ^{15}N-CP/MAS spectrum of DNP appeared at 183 ppm at 306 K and the peak strongly shifted toward the lower field 233 ppm (calibrated values as described later) when the temperature was decreased to 26 K as depicted in Fig. 3. The isotropic shift was distinguished from the spinning side bands by use of several spinning speeds as usual. The observed value 233 ppm for ^{15}N at lowest temperature is almost compatible with the non-protonated sp^2 nitrogen atom [10–12], indicating that the OH-form is more stable than the NH-form for the hydrogen bonds.

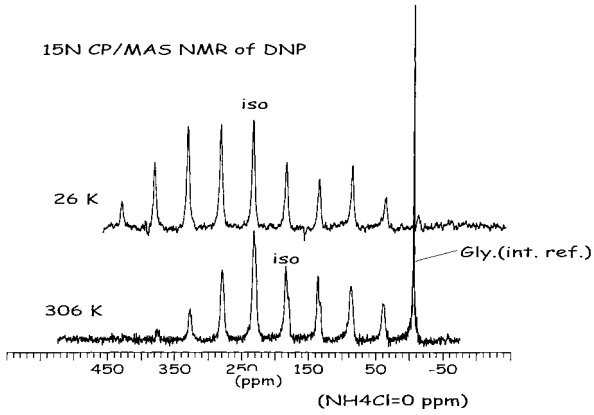

Fig. 3
^{15}N-CP/MAS NMR spectra of DNP measured with Bruker DSX 400 spectrometer and Doty Penguin Probe. The chemical shift was measured from ^{15}N-enriched NH_4Cl. ^{15}N-enriched glycine was used as an internal reference. The isotropic chemical shift was identified from the spinning side bands by using different spinning rates and is indicated by iso. The chemical shift was corrected (see into text, Sect. (3.1)). Small shoulder, which appeared above 224 K, was attributed to artificial origin, since the spectrum measured with Bruker CP/MAS probe at room temperature showed no shoulder

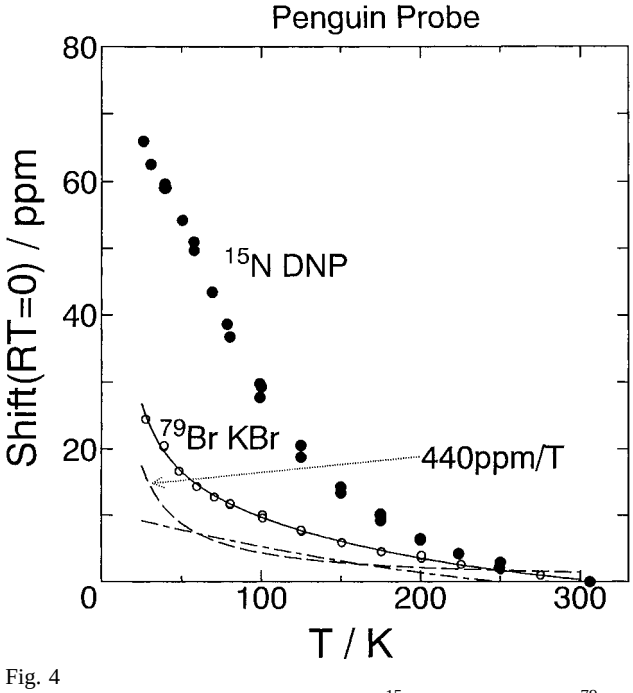

Fig. 4
Temperature dependence of the shift of ^{15}N of DNP and of ^{79}Br of KBr measured with Doty Penguin probe. The shift values are set to zero at 306 K. Solid curve is the best fit for the shift of ^{79}Br of KBr, showing the trial function that $\delta(^{79}\mathrm{Br}) = 10.73 + 439.9/T - 6.07\times10^{-2}\times T + 7.09\times10^{-5}\times T^2$ ppm. Broken curve is the second term $+439.9/T$ ppm which was attributed to the shift induced by paramagnetism of the probe, while chained curve represents the contribution of other terms of the above trial function

Unfortunately, the NMR lines of every sample measured with the Penguin probe exhibited artificial low field shift effect due to paramagnetism of a material used for constructing the probe. Thus the chemical shift data were corrected in the low temperature region. The low field shift

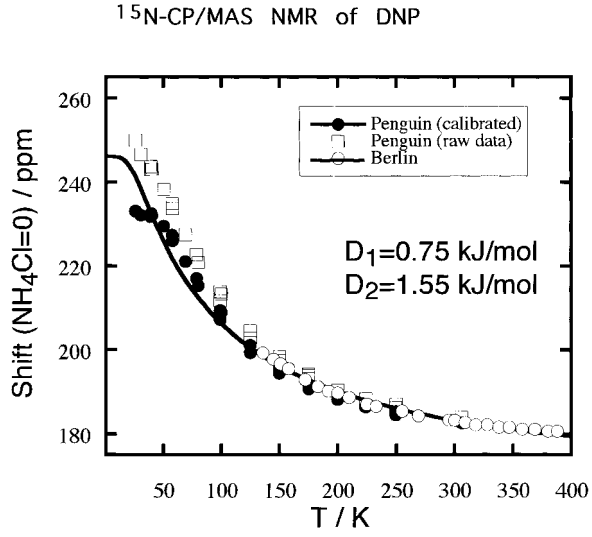

Fig. 5
Temperature dependence of ^{15}N chemical shift of DNP. □, raw data measured with Doty Penguin probe; ●, calibrated values of □ (see into text, Sect. (3.1)); ○, measured in Berlin with CP/MAS probe for conventional temperature region. Solid curve is the result of calculation based on the best compromise between ^{15}N chemical shift and T_1^{-1} of proton and the parameters are listed in the final column of Table 1. The shift was measured from ^{15}N-enriched NH_4Cl

was calibrated by using the shift of ^{79}Br spectrum of pulverized KBr sample under the same experimental conditions as those for DNP. The observed chemical shift of the ^{79}Br obeys a trial function, $\delta(^{79}\mathrm{Br}) = 10.73 + 439.9/T - 6.07\times10^{-2}\times T + 7.09\times10^{-5}\times T^2$ ppm as shown in Fig. 4, where raw data of the shifts $\delta(^{79}\mathrm{Br})$ of KBr and $\delta(^{15}\mathrm{N})$ of DNP were set to 0 ppm at 306 K and T is the absolute temperature. The second term $+439.9/T$ ppm, which dominates at very low temperature, is not expected for the diamagnetic KBr sample and was assumed to a contribution from a paramagnetic material of the Penguin probe. Magnetization of the paramagnetic material, which obeys Curie law, induces additional magnetic field at the sample position. Thus we subtracted the term of Curie law ($+439.9/T$ ppm) from the raw data of the chemical shift of ^{15}N-DNP in ppm scale and obtained the corrected shift (Fig. 5). The thermometer of the Penguin probe was not calibrated as described in the experimental section. However, the plot of all data showed no apparent gap between the shift values measured with the Penguin probe at IMS Japan and those with the probe equipped with the precisely calibrated thermometer in Berlin as shown in Fig. 5. Thus we used these shift values for an estimate of the set of energy differences among the tautomers. It is noted that the chemical shift varies largely below 100 K, suggesting the very small values of the energy differences.

3.2 ^{1}H-NMR Relaxation

The magnetization recovery curve was described by a single exponential function for all temperatures within experimental error. Thus, the spin temperature is established

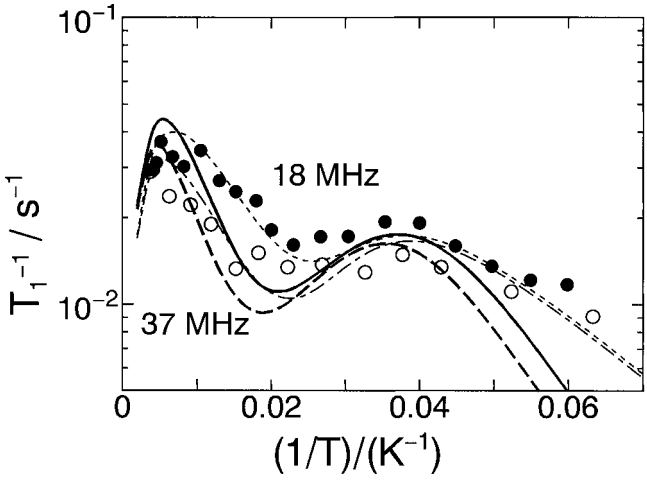

Fig. 6
Temperature dependence of the spin-lattice relaxation rate of proton of DNP: ●, measured at 18 MHz; ○, at 37 MHz. Solid and broken curves in bold type are the results of calculation for 18 and 37 MHz, respectively, based on the best compromise between T_1^{-1} of proton and ^{15}N chemical shift and the dynamic parameters obtained are listed in the final column of Table 1. Dotted (18 MHz) and chained (37 MHz) fine curves are the best independent fit to T_1^{-1} of proton (see into text, Sect. (5), and third column of Table 1)

between the proton in the hydrogen bond and other protons present in the crystal. The dynamics of proton in the hydrogen bond can be directly determined from the observed T_1^{-1} curve. The temperature dependence of the spin-lattice relaxation rate T_1^{-1} of proton of DNP at 18 and 37 MHz is shown in Fig. 6, in which two maxima of T_1^{-1} appeared near 25 and 200 K. Both maxima were assigned to the transfer motion of protons in the NHO hydrogen bonds. The observed frequency dependence of T_1^{-1} can not be explained by classical motion of proton and the slope of T_1^{-1} is very small. These results suggest the quantum mechanical tunneling of proton in the unequal double minimum potentials. This point is considered for the following model.

4. Model of Proton Transfer Dynamics in a Couple of Asymmetric NHO Hydrogen Bonds

In this section we construct a model for the analysis of temperature dependence of ^{15}N chemical shift and ^{1}H-NMR relaxation rate T_1^{-1}.

The combination of the two possible forms, the OH and NH forms, of the two hydrogen bonds in a DNP molecule may lead to four tautomeric forms, i.e. {OH, OH}, {OH, NH}, {NH, OH} and {NH, NH}, which are numbered I through IV in order as shown in Fig. 7. Two of the four tautomers, {OH, NH}, and {NH, OH} are probably the same or very closely located in energy even in the solid state, since a crystallographical inversion symmetry exists at the center of the molecule [6]. The differential Fourier map of X-ray diffraction indicates the delocalization of proton and slightly large population for the OH form [6]. The OH form is more stable state than the NH form, which is consistent with the observation of the chemical shift of ^{15}N described above. The model of proton transfer dynamics given in Fig. 7 is, therefore, employed. In this model, the two tautomers, {OH, NH} and {NH, OH} are assumed to be degenerate in energy, and there are three energetically different states. The proton dynamics in DNP can be expressed by two kinds of reaction coordinates u_1 and u_2 as shown in Fig. 7. The figure depicts a double minimum potential for each reaction coordinate together with tunneling rates, k_1 and k_2, and classical jumping rates, α and β. The proton tunneling in DNP is a similar phenomenon to that in carboxylic acid dimers and we employed the phonon-assisted tunneling model proposed by Skinner and Trommsdorff [13].

4.1 Temperature Dependence of the ^{15}N Chemical Shift

A single and sharp signal was observed for DNP in all temperature region investigated as described in Sect. 3.1. The exchange rate is much larger than the difference of the chemical shifts of four tautomers. In this case the averaged shift δ_{avd} for each of the two nitrogen is given by,

$$\delta_{\mathrm{avd}} = \delta_{\mathrm{I}}\, x_{\mathrm{I}} + \delta_{\mathrm{II}}\, x_{\mathrm{II}} + \delta_{\mathrm{III}}\, x_{\mathrm{III}} + \delta_{\mathrm{IV}}\, x_{\mathrm{IV}}\,, \tag{1}$$

where

$$x_{\mathrm{I}} + x_{\mathrm{II}} + x_{\mathrm{III}} + x_{\mathrm{IV}} = 1\,. \tag{2}$$

The quantities δ_{i} and x_{i}(i=I through IV) are the chemical shift and relative populations for the different tautomers I through IV shown in Fig. 7. Supposing that OH- and NH-form of the hydrogen bond respectively give the same shift even in the different tautomers, we obtain,

$$\delta\,(\mathrm{A})_{\mathrm{avd}} = \delta_{\mathrm{OH}}\, x_{\mathrm{I}} + \delta_{\mathrm{OH}}\, x_{\mathrm{II}} + \delta_{\mathrm{NH}}\, x_{\mathrm{III}} + \delta_{\mathrm{NH}}\, x_{\mathrm{IV}} \tag{3}$$

and

$$\delta\,(\mathrm{B})_{\mathrm{avd}} = \delta_{\mathrm{OH}}\, x_{\mathrm{I}} + \delta_{\mathrm{NH}}\, x_{\mathrm{II}} + \delta_{\mathrm{NH}}\, x_{\mathrm{III}} + \delta_{\mathrm{OH}}\, x_{\mathrm{IV}}\,, \tag{4}$$

respectively, for the two nitrogen atoms N_A (right hand side of the molecule in Fig. 7) and N_B (left hand side) in a molecule. X-ray diffraction experiment indicated the inversion symmetry to exist at the center of the molecule, suggesting that two of the four tautomers II and IV are equivalent or very closely located in energy. We also assume that $x_{\mathrm{II}}=x_{\mathrm{IV}}$ and $\delta_{\mathrm{II}}=\delta_{\mathrm{IV}}$ both for the OH-form and NH-form for the simplicity. Then following relation can be obtained for the shift of the observed signal, δ_{obs},

$$\begin{aligned}\delta_{\mathrm{obs}} &= \delta\,(\mathrm{A})_{\mathrm{avd}} = \delta\,(\mathrm{B})_{\mathrm{avd}} \\ &= \delta_{\mathrm{OH}}\, x_{\mathrm{I}} + (\delta_{\mathrm{OH}} + \delta_{\mathrm{NH}})\, x_{\mathrm{II}} + \delta_{\mathrm{NH}}\, x_{\mathrm{III}} \\ &= \frac{\delta_{\mathrm{OH}}\,(1 + \mathrm{e}^{-D_1/RT}) + \delta_{\mathrm{NH}}\,\mathrm{e}^{-D_1/RT}\,(1 + \mathrm{e}^{-D_2/RT})}{1 + \mathrm{e}^{-D_1/RT}\,(2 + \mathrm{e}^{-D_2/RT})}\end{aligned} \tag{5}$$

where D_1 and D_2 are the energy differences between I and II (IV) and between II (IV) and III, respectively, as shown in Fig. 7. The notation of OH-form corresponds to non-protonated sp^2 nitrogen atom of which the intrinsic chemical shift is designated as δ_{OH}, while NH-form corresponds to sp^3 nitrogen atom and the intrinsic chemical shift is designated by δ_{NH}.

4.2 Derivation of the Formula of T_1^{-1} for the Four-Site Exchange in Unequal Potential Wells

The spin-lattice relaxation of the proton in the hydrogen bond is dominated by the dipole interaction between the proton (I spin) and ^{14}N nucleus (S spin), because the distance between H and N in the hydrogen bond is very short compared with the distances between the proton in the hydrogen bond and other protons present in the crystal. The spin-lattice relaxation formula for the proton dynamics in the unequal potential wells is derived from the general expression of the spin relaxation [14–20]. Details of the formulation are described in Appendix in the last section of this paper.

The spin-lattice relaxation rate of proton (I spin) is given by,

$$T_1^{-1}(\mathrm{II}) = m \cdot \gamma_N^2 \gamma_H^2 \cdot S(S+1) \cdot \sum_{l=1}^{3} A_{l,HN} \cdot B_{II}^{(1)}(\tau_l), \quad (6)$$

here the function $B^{(1)}(\tau_l)$ is the power spectrum for unlike spins and is described by [21, 22]

$$B_{II}^{(1)}(\tau_l) = J(\tau_l, \omega_H - \omega_N) + 3J(\tau_l, \omega_H) + 6J(\tau_l, \omega_H + \omega_N) \quad (7)$$

and

$$J(\tau, \omega) = \tau/(1 + \tau^2 \omega^2). \quad (8)$$

The coefficient m in Eq. (6) denotes the fraction of the proton spins that directly relax due to the motion among all the proton spins present in the crystal. The value m equals 2/20 for DNP. S is the nuclear spin of ^{14}N ($S=1$). Notations ω_H and ω_N are the Larmor frequencies of the proton and ^{14}N, respectively. Here we neglected the effect of nuclear quadrupole splitting of ^{14}N. The detailed derivation of Eq. (6) and expression of the coefficients $A_{l,HN}$ are presented in Appendix (the coefficient $A_{l,HN}$ is represented by A_l in Appendix for generalities).

There are three kinds of relaxation correlation times, τ_1, τ_2 and τ_3, all of which are functions of classical jumping rates (a, β, a' and β'), tunneling rates (k_1, k_2, k_1' and k_2'), and population differences (P, Q),

$$\begin{aligned}
\tau_1^{-1} &= PW_1 + W_2 \\
\tau_2^{-1} &= \frac{1}{2}\{(P+2)W_1 + (2Q+1)W_2 + S\} \\
\tau_3^{-1} &= \frac{1}{2}\{(P+2)W_1 + (2Q+1)W_2 - S\}
\end{aligned} \quad (9)$$

where

$$\begin{aligned}
P &= \exp(D_1/RT) \\
Q &= \exp(D_2/RT) \\
S &= \sqrt{\{(P+2)W_1 + (2Q+1)W_2\}^2 - 8W_1W_2(PQ+2Q+1)}.
\end{aligned} \quad (10)$$

The transition rates (proton transfer rates) from stable to metastable state, W_1 and W_2, can be approximated by a sum of classical jumping rates, a and β, and tunneling rates, k_1 and k_2 [13],

$$\begin{aligned}
W_1 &= a + k_1 \\
&\quad (\text{for } \{OH,OH\} \rightarrow \{OH,NH\}, \\
&\qquad \{OH,OH\} \rightarrow \{NH,OH\}) \\
W_2 &= \beta + k_2 \\
&\quad (\text{for } \{OH,NH\} \rightarrow \{NH,NH\}, \\
&\qquad \{NH,OH\} \rightarrow \{NH,NH\})
\end{aligned} \quad (11)$$

where

$$\begin{aligned}
a &= a_0 \exp(-A_1/RT), \\
\beta &= \beta_0 \exp(-A_2/RT), \\
k_1 &= k_{10}/\{\exp(D_1/RT) - 1\}, \\
k_2 &= k_{20}/\{\exp(D_2/RT) - 1\}.
\end{aligned} \quad (12)$$

The reverse transfer rates are expressed as follows,

$$\begin{aligned}
W_1' &= a' + k_1' \\
&\quad (\text{for } \{OH,NH\} \rightarrow \{OH,OH\}, \\
&\qquad \{NH,OH\} \rightarrow \{OH,OH\}), \\
W_2' &= \beta' + k_2' \\
&\quad (\text{for } \{NH,NH\} \rightarrow \{OH,NH\}, \\
&\qquad \{NH,NH\} \rightarrow \{NH,OH\}),
\end{aligned} \quad (13)$$

where

$$\begin{aligned}
a' &= aP, \\
\beta' &= \beta Q, \\
k_1' &= k_1 P, \\
k_2' &= k_2 Q.
\end{aligned} \quad (14)$$

Relations in Eq. (14) satisfy the detailed balance condition. The quantities A_1 and A_2 express the potential barrier hight in the limit of classical approximation, whereas they represent the activation energies in practice. The origin of the potential barrier for the proton transfer in the solid state is closely related to what is the reaction coordinate for the proton transfer motion in the hydrogen bond in the solid state. The substance of the observable activation energy has not yet been claified but is being in discussion.

Table 1
Parameters of proton transfer in the hydrogen bond of DNP for the calculations of the chemical shift of ^{15}N and the spin-lattice relaxation rate of proton

		^{15}N-Chemical shift (best independent fit)	^{1}H-Relaxation (best independent fit)	^{1}H-Relaxation and ^{15}N-Chemical shift (best compromise)
Energy difference	D_1	1.4 kJ/mol	0.4 kJ/mol	0.75 kJ/mol
	D_2	0.3 kJ/mol	0.9 kJ/mol	1.5 kJ/mol
Activation energy	A_1	–	2 kJ/mol	2 kJ/mol
	A_2	–	10 kJ/mol	8 kJ/mol
Classical rate	α_0	–	4×10^{11} s^{-1}	1×10^{11} s^{-1}
	β_0	–	1×10^{9} s^{-1}	1×10^{9} s^{-1}
Tunneling	k_{10}	–	1.1×10^{9} s^{-1}	3.0×10^{8} s^{-1}
	k_{20}	–	9.0×10^{7} s^{-1}	1.0×10^{8} s^{-1}
NH distance[a])	OH-form	–	0.159 nm	0.159 nm
	NH-form	–	0.113 nm	0.110 nm
^{15}N Chemical shift[b])	OH-form	235 ppm	271 ppm	246 ppm
	NH-form	107 ppm	73 ppm	87 ppm

[a]) The distribution of hydrogen atom in the NHO hydrogen bond was found by X-ray diffraction experiment. But the coordinate is not so precise that we can calculate the dipole interaction accurately. The shorter NH distance was chosen to fit the observed T_1^{-1} maximum within the experimental error of the X-ray diffraction.
[b]) ^{15}N chemical shift was measured from ^{15}N-NH_4Cl. The chemical shift of ^{15}N-NH_4Cl is located at –341.15 ppm from liquid nitromethane.

The coefficient $A_{l,\mathrm{HN}}$ is the structure-dependent term of the dipole interaction and the term which is a function of the transition rate and the population differences among the tautomers (Appendix). This coefficient was calculated by using the structural parameters of the NHO hydrogen bond. The distribution of hydrogen atom in the NHO hydrogen bond was found by X-ray diffraction experiment. But the coordinate is not so precise that we can calculate the dipole interaction accurately. The value of $A_{l,\mathrm{HN}}$ sensitively depends on the shorter NH distance (r_{NH}) and is nearly proportional to r_{NH}^{-6}. Thus the shorter NH distance was chosen to fit the observed T_1^{-1} maximum within the range of experimental error of the X-ray diffraction. We used the NH distance of 0.159 nm for the OH form and the angle of 5°, which is determined by the two N → H vectors of the OH and NH forms of the hydrogen bond. The NH distance of 0.110 or 0.113 nm was used for the NH form depending on the fitting procedures (Table 1). These parameters are consistent with the crystal structure of DNP [6].

Before discussing the calculation of T_1^{-1} and the proton transfer dynamics in the DNP crystal, we shortly comment the three kinds of correlation times of the spin relaxation given in Eq. (9). If we consider the limiting case that $W_1 \gg W_2$, i.e. the proton transfer {OH, OH}↔{OH, NH} and {OH, OH}↔{NH, OH} are much faster than {OH, NH}↔{NH, NH} and {NH, OH}↔{NH, NH}, the correlation tims can be approximated by simple forms,

$$\begin{aligned}\tau_1^{-1} &\approx P W_1 \\ \tau_2^{-1} &\approx (P+2)\, W_1 \\ \tau_3^{-1} &\approx \frac{1}{2}\,(2Q+1)\, W_2 \,. \end{aligned} \tag{15}$$

Then the following relation holds,

$$\tau_1^{-1} \approx \tau_2^{-1} \gg \tau_3^{-1} \,. \tag{16}$$

Therefore two maxima of T_1^{-1} are separately observed in this case. We used the original formula in Eq. (9) for the correlation times to calculate the T_1^{-1} of DNP.

5. Discussion

The energy differences among the tautomers of DNP, D_1 and D_2, depicted in Fig. 7 were estimated by least-squared fitting of Eq. (1) to the temperature dependence of the chemical shift of ^{15}N plotted in Fig. 5. Free fitting procedure leads to several sets of four parameters, δ_{OH}, δ_{NH}, D_1 and D_2. The corrected chemical shift seems to converge at about 235 ppm in the low temperature limit. Supposing that the intrinsic chemical shift of non-protonated nitrogen atom δ_{OH} can be fixed to 235 ppm, the best fitting gave the energy differences, $D_1 = 1.4$ kJ/mole and $D_2 = 0.3$ kJ/mole, and the chemical shift of protonated nitrogen atom $\delta_{\mathrm{NH}} = 107$ ppm [8]. The fitting error is 0.1 kJ/mol for D_1 and D_2 and 2 ppm for δ_{NH}. It is noteworthy that the energy differences among the tautomers of DNP are very small in spite of the fact that the tautomerism is accompanied with the proton transfer in the chemically asymmetric NHO hydrogen bonds. For most of compounds with NHO hydrogen bonds reported hitherto, the hydrogen atom is strongly trapped at the oxygen atom site. The very small energy difference between the OH- and NH-form of the hydrogen bond is a remarkable property of DNP molecule in the crystalline state.

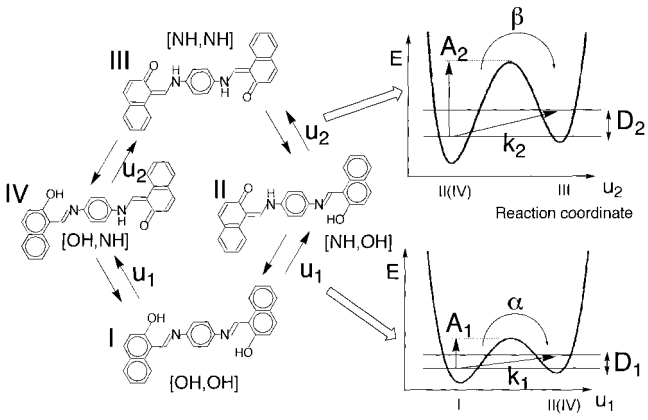

Fig. 7
Elementary processes of the tautomerism and a model of proton transfer in the hydrogen bonds of DNP

Calculation of T_1^{-1} of proton by Eqs. (6) through (14) gave a good fitting to the observed temperature and frequency dependence. It was concluded that the broad maximum of T_1^{-1} near 25 K is mainly induced by the transitions {OH, OH}↔{OH, NH} and {OH, OH}↔{NH, OH}, while the maximum of T_1^{-1} near 200 K is induced by the transitions {OH, NH}↔{NH, NH} and {NH, OH}↔{NH, NH}. The best fitting for the T_1^{-1} of proton is shown by dotted and chained fine curves for 18 and 37 MHz, respectively and the derived parameters of the proton transfer motion are listed in the fourth column of Table 1. The energy differences of $D_1 = 0.4$ kJ/mol and $D_2 = 0.9$ kJ/mol were obtained [23]. These values are slightly different from those estimated independently from the chemical shift of ^{15}N, i.e. $D_1 = 1.4$ kJ/mol and $D_2 = 0.3$ kJ/mol. If we use the latter values for calculating the T_1^{-1}, the maximum of T_1^{-1} near 25 K could never be reproduced. It should be noticed that we employed the models as simple as possible both for the analysis of the chemical shift and for T_1^{-1}. An additional mechanism of the proton transfer motion, which was not taken into account at present, may lead to a set of common parameters for better fittings of the theoretical curves to the observed proton T_1^{-1} and ^{15}N chemical shift. A possible mechanism is the direct exchange between the two equivalent tautomers, II and IV, in Fig. 7. Since there is no energy difference between the two tautomers, tunneling effect becomes a driving force to induce the direct exchange between II and IV. The direct exchange process gives an additional spin-lattice relaxation of proton, whereas this exchange induces no effect on the temperature dependence of the chemical shift of ^{15}N. To include the direct exchange process, the number of adjustable parameters increases. Thus we confine ourselves at present to the model as simple as possible. Within the framework of the present model, the energy scheme and the parameters of the proton dynamics were determined on the basis of compromise of the two fittings for the proton T_1^{-1} and for the ^{15}N chemical shift. The result of the calculation of the temperature dependence of the chemical shift of ^{15}N is shown by the solid curve in Fig. 5. The solid and the broken curves in bold type depict the calculations of T_1^{-1} of proton for 18 and 37 MHz, respectively, in Fig. 6. The common parameters used are summarized in the final column of Table 1.

The derived rate constants of proton tunneling in the crystalline state of DNP are comparable to those reported for several carboxylic acid dimers in the solid state [13, 24–26]. It is interesting to compare the two different systems. In the case of carboxylic acid dimers such as benzoic acid, the two proton tautomers are equivalent in the isolated state, whereas the proton is trapped in one of the two configurations in the crystalline phase due to the anisotropy of the crystalline field. A balance between the destabilization due to the molecular deformation and the stabilization due to the lattice energy determines the energy difference between the two tautomers. On the other hand, it is considered for the molecule with the chemically asymmetric NHO hydrogen bonds that major part of the energy difference among the tautomers is controlled by the π-electron structure of the molecule. The NH-form of the hydrogen bond of DNP is considerably stabilized compared with other compound with NHO hydrogen bonds. For example, N,N′-bis(salicylidene)-p-phenylenediamine (BSP) exhibited much larger energy differences among the tautomers [8]. In addition to the remarkable character of stabilization of the NH form of the hydrogen bond in the solid DNP, the following result should be noted.

The two activation energies A_1 and A_2 of proton transfer in NHO hydrogen bonds of DNP are significantly different from each other as shown in Table 1. This result suggests a significant interaction between the two hydrogen bonds in different part of a molecule. In the first process shown in the lower part of Fig. 7, the proton in one hydrogen bond transfers from the oxygen to the nitrogen atom, during the other hydrogen bond is the “OH-form”. The value of A_1 is 2 kJ/mol. On the other hand, in the second process shown in the upper part of Fig. 7, the proton transfer from the oxygen to the nitrogen atom, which is the same as in the first process, but in the second process the other hydrogen bond is the “NH-form”. This situation is different from the first process. The activation energy A_2 is almost 8 kJ/mol, which is much larger than A_1 (= 2 kJ/mol). The potential energy function of the proton transfer motion in one hydrogen bond remarkably depends on what is the form of the other hydrogen bond, i.e. OH- or NH-form. If there is no interaction between the two protons in different parts of a molecule, the energy values and the rate constants for the proton transfer should never be different between the upper and the lower processes in Fig. 7. This type of interaction between the hydrogen bonds is very interesting in the viewpoint of information transfer. The information, i.e. OH-form or NH-form, of one hydrogen bond propagates to the second hydrogen bond and the potential function for the proton transfer in the second hydrogen bond is changed.

The authors are grateful to Drs. H. Ogata, D. Kuwahara and T. Mochida and Prof. S. Miyajima of Institute for Molecular Science for their support of the installation of Penguin Probe. This research was supported in part by the grant-in-aid to S.T. from the Ministry of Science, Education, Sports, and Culture of Japan (Nos. 09640681 and 10146212).

Appendix

The formulation that we apply to the four-site exchange process in unequal potential wells is based on an equation of motion with stochastic probability that governs the exchange processes among the allowed states. The number of energetically nonequivalent states to be taken into account is not limited in this treatment and the spin relaxation formula for complicated multi-site exchange processes in unequal potential wells can be easily formulated. The formulation neglects the so-called "cross correlation effect" [27, 28] or "symmetry restricted spin diffusion" [29, 30] in spin relaxation. The cross correlation is important for symmetrically arranged multi-spins such as methyl group, ammonium ion, and methane molecule, etc. On the other hand, the cross correlation effect is not important in the case of the hydrogen-bonded system. Thus the present formulation is correct. The formalism was presented by Prof. Gen Soda of Institute for Molecular Science, Japan at first. Only a part of his work was published [16, 18–20], since he suddenly died in 1980 before the full paper was completed. In this appendix his formalism is presented particularly for the motion in unequal potential wells in Sects. (A1) and (A2). His manuscript was partially rearranged from the viewpoint of recent developments. The formalism is applied to our DNP system in Sect. (A3).

A.1 General Method for Formulating the Spin Relaxation Induced by Molecular and Atomic Motions in Equal and Unequal Potential Wells

For an isolated dipolar coupled two spins with $I=1/2$, the spin-lattice relaxation rate is give by [31]

$$\frac{1}{T_1}=\frac{9}{4}\,\gamma^4\,\hbar^2\left\{J^{(1)}\left(\omega_0\right)+J^{(2)}\left(2\,\omega_0\right)\right\}, \tag{A1}$$

for like-spin and by

$$\frac{1}{T_1^{\mathrm{I}}}=\gamma_{\mathrm{I}}^2\,\gamma_{\mathrm{S}}^2\,\hbar^2\,S\left(S+1\right) \times\left\{\frac{1}{12}\,J^{(0)}(\omega_{\mathrm{I}}-\omega_{\mathrm{S}})+\frac{3}{2}\,J^{(1)}(\omega_{\mathrm{I}})+\frac{3}{4}\,J^{(2)}(\omega_{\mathrm{I}}+\omega_{\mathrm{S}})\right\} \tag{A2}$$

for I spin coupled with unlike-spin S [21]. In general we have to consider the coupled equation for the spin relaxation in the case of dipolar coupled unlike-spin system [21].

However in our case of DNP, the magnetization of ^{14}N spins is very small compared with that of ^{1}H spins. In this case, the cross relaxation term of the coupled equation gives a negligible contribution to the relaxation of proton magnetization and the proton magnetization can be approximated by a single exponential function as we mentioned in Sect. (3.2). On the contrary, cross relaxation effect will affect spin relaxation of ^{15}N particularly for the cross-polarization experiment.

The power spectra $J^{(\mathrm{m})}(\omega)$ of the fluctuating random part ($f^{(\mathrm{m})}(t)$) of the dipole coupling tensor ($F^{(\mathrm{m})}(t)$) are defined by the Fourier transform of the correlation functions,

$$g_{\mathrm{m}}\left(\tau\right)=\left\langle f^{(\mathrm{m})}\left(\tau\right)^* f^{(\mathrm{m})}\left(t-\tau\right)\right\rangle$$

$$J^{(\mathrm{m})}\left(\omega\right)=\mathrm{Re}\int_0^\infty \mathrm{d}\tau\left(\mathrm{e}^{\mathrm{i}\omega\tau}\,g_{\mathrm{m}}\left(\tau\right)\right)=\frac{1}{2}\int_{-\infty}^{\infty}\mathrm{d}\tau\left(\mathrm{e}^{\mathrm{i}\omega\tau}\,g_{\mathrm{m}}\left(\tau\right)\right) \tag{A3}$$

where $\langle\cdots\rangle$ means the thermal averaging over an ensemble of spin systems and

$$f^{(\mathrm{m})}\left(t\right)=F^{(\mathrm{m})}\left(t\right)-\left\langle F^{(\mathrm{m})}\left(t\right)\right\rangle. \tag{A4}$$

The power spectra satisfy the relation

$$J^{(\mathrm{m})}\left(\omega\right)=J^{(\mathrm{m})}\left(\omega\right)^*=J^{(-\mathrm{m})}\left(-\omega\right) \tag{A5}$$

which is proved from the symmetry relation of the correlation functions

$$g_{\mathrm{m}}\left(\tau\right)=g_{\mathrm{m}}\left(-\tau\right)^*=g_{-\mathrm{m}}\left(-\tau\right). \tag{A6}$$

The auto-correlation function of $F^{(\mathrm{m})}(t)$ is

$$G_{\mathrm{m}}\left(t\right)=\left\langle F^{(\mathrm{m})}\left(0\right)F^{(\mathrm{m})}\left(t\right)^*\right\rangle. \tag{A7}$$

In the case of powdered crystals or liquids, simplification arises from the spatial averaging over all possible orientations of the crystallographic axes relative to the applied magnetic field. The power spectra was proven to satisfy [22]

$$J^{(0)}\left(\omega\right)=J^{(1)}\left(\omega\right)=J^{(2)}\left(\omega\right), \tag{A8}$$

irrespective of the modes of motion responsible for the spin relaxation, although the analytical expressions of $f^{(\mathrm{m})}(t)$, and accordingly $g_{\mathrm{m}}(t)$, depend on the mode of motion modulating the dipole coupling.

In the next step, a formulation is given of the auto-correlation functions, $G_{\mathrm{m}}(t)$, and their Fourier transform, power spectra $J^{(\mathrm{m})}(\omega)$, for general model of the motion. The central objective of this work is to calculate the correlation functions $G_{\mathrm{m}}(t)$ or the power spectra $J^{(\mathrm{m})}(\omega)$ on an appropriate stochastic model for the motion. In typical crystals, atoms and molecules vibrate or librate about the potential minima of quasi-equilibrium positions or orientations for some period of time before jumping to other position or orientation. This jump is assumed to be stochastic. Except for the coherent rotational tunneling [32, 33], the spin relaxation due to motions of atoms and molecules has been treated by stochastic model even for the phonon-assisted proton tunneling in unequal double minimum potential wells [13]. It is noted that the jumps are assumed to be instantaneous so that the atom position and molecular orientation are always at one of the quasiequilibrium sites. The residence time is much longer than the time needed for a jump from one site to another. This kind of motion might be well described as Markovian, characterized by the transition probabilities $P_{\mathrm{jk}}(t)$. $P_{\mathrm{jk}}(t)$ expresses the probability that a given inter spin vector which was at a site j will be found at another site k after the time t. Supposing that the number of possible sites is finite and that the time-dependent random dipole coupling tensor $F(t)$ takes on anyone of n discrete values (F_1, F_2,$\cdots$, F_{n}) corresponding to the n different sites of the internuclear vector, the auto-correlation function of $F(t)$ in the thermodynamic equilibrium state is written in terms of the transition probabilities $P_{\mathrm{jk}}(t)$,

$$G\left(t\right)=\left\langle F\left(0\right)F\left(t\right)^*\right\rangle=\sum_{\mathrm{j,\,k}}P_{\mathrm{j}}^0\,F_{\mathrm{j}}\,P_{\mathrm{jk}}\left(t\right)F_{\mathrm{k}}^*, \tag{A9}$$

where the initial distribution over the sites is described by the weights ($P_1^0, P_2^0, \cdots, P_{\mathrm{n}}^0$) and sum is taken over all possible pairs of sites. The jumping of a internuclear vector from the site j to the site k is described by the transition probability $P_{\mathrm{jk}}(t)$ which only depends on the time interval t,

$$P_{\mathrm{jk}}\left(t\right)=\sum_{\mathrm{m}}P_{\mathrm{jm}}\left(t-\tau\right)\cdot P_{\mathrm{mk}}\left(\tau\right) \tag{A10}$$

Assuming that for small $t(t \geq 0)$,

$$P_{jj}(t) = 1 - t/\tau_j\,,$$
$$P_{jk}(t) = p_{jk} \cdot t/\tau_j \,(j \neq k)\,, \tag{A11}$$

the Chapman-Kolmogolov equation is rewritten in the form of differential equation,

$$\dot{P}_{jk}(t) = -P_{jk}(t)/\tau_k + \sum_{m\,(\neq k)} P_{jm}(t)\, p_{mk}/\tau_m\,, \tag{A12}$$

where τ_j is the residence time at the side j and p_{jk} is the conditional transition probability of the event that if a jump from site j occurs during a small time interval t then it will take the system from site j to k in a unit time satisfying

$$\sum_{k\,(\neq j)} p_{jk} = 1\,. \tag{A13}$$

Defining the matrix $\boldsymbol{P}(t)=(P_{jk}(t))$ and the transition matrix $\boldsymbol{D}$,

$$D_{jj} = \frac{1}{\tau_j}\,, \quad D_{jk} = -\frac{p_{jk}}{\tau_j}\,(j \neq k)\,, \tag{A14}$$

the differential Eq. (A12) is rewitten in a form of

$$\dot{\boldsymbol{P}}(t) = -\boldsymbol{P}(t)\,\boldsymbol{D}\,. \tag{A15}$$

We define a row vector $\boldsymbol{\xi}_0 = (P_1^0, P_2^0, \cdots, P_n^0)$ where P_i^0 is the fractional occupation at the site i under thermal equilibrium. The vector $\boldsymbol{\xi}_0$ is a unique solution of the equation that

$$\boldsymbol{\xi}_0\,\boldsymbol{D} = \boldsymbol{0}\,. \tag{A16}$$

Defining the column vector η_0,

$$\boldsymbol{\eta}_0 = \begin{pmatrix} 1 \\ 1 \\ \cdot \\ \cdot \\ 1 \end{pmatrix}, \tag{A17}$$

the normalization of the equilibrium distribution P_j^0 is expressed by

$$\sum_j P_j^0 = \boldsymbol{\xi}_0\,\boldsymbol{\eta}_0 = 1 \tag{A18}$$

and

$$\boldsymbol{D}\boldsymbol{\eta}_0 = \boldsymbol{0}\,. \tag{A19}$$

A usual practice in defining the transition matrix $\boldsymbol{D}$ is to assume a microscopic reversibility between the sites j and k,

$$P_j^0\, D_{jk} = P_k^0\, D_{kj}\,, \tag{A20}$$

in other words, the Onsager's reciprocal relation for transition probabilities or the principle of detailed balance between the two connecting sites. This means that if we use the matrix $\boldsymbol{d}$ connected to $\boldsymbol{D}$ by a similarity transformation $\boldsymbol{V}$,

$$V_{ij} = \frac{1}{\sqrt{P_i^0}} \cdot \delta_{ij}$$
$$\boldsymbol{d} = \boldsymbol{V}^{-1}\,\boldsymbol{D}\boldsymbol{V} \qquad \text{or}$$
$$d_{ij} = \sqrt{P_i^0} \cdot D_{ij} \cdot \frac{1}{\sqrt{P_i^0}}\,, \tag{A21}$$

it serves in place of $\boldsymbol{D}$, because $\boldsymbol{d}$ is symmetric and has a set of eigenvalues identical to that of the matrix $\boldsymbol{D}$. It is easily proved that $\boldsymbol{d}$ is non-negative (positive semi-definite) and the rank is (*n*–1). The matrix $\boldsymbol{d}$ can be diagonalized into the eigen value matrix, $\Lambda(\Lambda_1 = 0 < \Lambda_2 < \Lambda_3 < \cdots < \Lambda_n)$ by a unitary transformation $\boldsymbol{U}$,

$$\boldsymbol{U}\boldsymbol{\Lambda} = \boldsymbol{d}\boldsymbol{U}\,. \tag{A22}$$

Eqs. (A16) and (A19) are equivalent with

$$\boldsymbol{d}\boldsymbol{V}^{-1}\,\boldsymbol{\eta}_0 = \boldsymbol{0} \tag{A23}$$

therefore

$$U_{i1} = \sqrt{P_i^0}\,. \tag{A24}$$

The formal solution of Eq. (A15) with initial condition $\boldsymbol{P}(t=0)=\boldsymbol{E}$ (unit matrix) is easily found to be

$$\boldsymbol{P}(t) = \mathrm{e}^{-\boldsymbol{D}t} = \boldsymbol{V}\cdot\boldsymbol{U}\cdot\mathrm{e}^{-\boldsymbol{\Lambda}t}\cdot\tilde{\boldsymbol{U}}^*\cdot\boldsymbol{V}^{-1} \tag{A25}$$

where $\tilde{\boldsymbol{U}}$ means the transposed matrix of $\boldsymbol{U}$. Therefore the *n*-site exchange process can be described by a set of (*n*–1) eigen values though some may be equivalent in some cases [18].

From Eq. (A9) the auto-correlation function $G(t)$ is now given by

$$G(t) = \boldsymbol{\xi}_0\,\boldsymbol{F}\boldsymbol{P}(t)\,\boldsymbol{F}^*\,\boldsymbol{\eta}_0$$
$$= \tilde{\boldsymbol{\eta}}_0\,\boldsymbol{V}^{-1}\,\boldsymbol{F}\boldsymbol{U}\mathrm{e}^{-\boldsymbol{\Lambda}t}\,\tilde{\boldsymbol{U}}^*\,\boldsymbol{F}^*\,\boldsymbol{V}^{-1}\,\boldsymbol{\eta}_0\,, \tag{A26}$$

where $\boldsymbol{F}$ means the diagonal matrix with the elements $F_{ij}=F_i\delta_{ij}$.

Eq. (A24) shows that the contribution of the term with $\Lambda_1=0$ to the correlation function $G(t)$ is given by the squared ensemble average of the random variable $F(t)$,

$$\langle F(t)\rangle = \boldsymbol{\xi}_0\,\boldsymbol{F}\,\boldsymbol{\eta}_0\,. \tag{A27}$$

Therefore the auto-correlation function of the fluctuating part of the dipole coupling tensor defined by Eq. (A4), which is responsible for the spin relaxation, is given by

$$\langle f(0) f(t)^*\rangle = \langle F(0)\,F(t)^*\rangle - |\langle F(t)\rangle|^2$$
$$= \sum_{k\,(\neq 1)} \mathrm{e}^{-\Lambda_k t} \sum_{i,j} \sqrt{P_i^0}\,\sqrt{P_j^0}\,U_{ik}\,U_{jk}^*\,F_i\,F_j^* \tag{A28}$$

In case of powdered crystals, the power spectra become independent of *m* (Eq. A8) after the spatial averaging,

$$\overline{F_i^{(m)}\,F_j^{*(m)}} = \frac{2}{15}\,\frac{1}{r_i^3\,r_j^3}\,P_2(\cos\Omega_{ij})\,, \tag{A29}$$

where $P_2(z)=(3z^2-1)/2$ is the Legendre polynominal and Ω_{ij} designates the mutual angle between the direction of the inter-nuclear vector at the site i and that at the site j. The value r_i represents the inter-nuclear distance at the site i. Defining the factor A_l, which depends on the geometry of the system, and the correlation time τ_{cl} of the *l*-th "normal mode" of spin relaxation by

$$A_l = \frac{2}{15}\sum_{i,j}\sqrt{P_i^0}\,\sqrt{P_j^0}\cdot\left(\sum_k{}' U_{ik}\,U_{jk}^*\right) r_i^{-3}\,r_j^{-3}\,P_2(\cos\Omega_{ij}) \tag{A30}$$

where the summation over k is taken for the same eigen values $\Lambda_l^{-1}(l \neq 1;\ \Lambda_l^{-1} = 0)$, and

$$\tau_{cl} = \Lambda_l^{-1}\,(l \neq 1)\,, \tag{A31}$$

the spin relaxation rate is expressed by

$$T_1^{-1} = C \sum_l A_l \cdot B(\tau_{cl}) \tag{A32}$$

where for like-spin systems with 1/2 spin $C = \frac{9}{4}\gamma^4\hbar^2$ and $B(\tau_c)$ is independent of the modes of atomic or molecular motion and is defined by

$$B(\tau_c) = j(\lambda_c, \omega) + 4j(\lambda_c, 2\omega), \tag{A33}$$

where

$$j(\lambda_c, \omega) = \mathrm{Re}\int_0^\infty e^{i\omega t} e^{-t/\tau_c} dt = \frac{\lambda_c^2}{\lambda_c^2 + \omega^2}, \quad (\lambda_c = \tau_c^{-1}). \tag{A34}$$

The particular nature of molecular or atomic motion is manifested in the factor A_l and the correlation time τ_{cl}.

It is worth noting that [22]

$$\sum_l CA_l = C\langle[f^{(0)}(t)]^2\rangle = \frac{2}{3}(M_2^{rigid} - M_2^\infty) \tag{A35}$$

where M_2^{rigid} is the second moment of the resonance line shape [34],

$$M_2^{rigid} = \frac{3}{2} C\langle[F^{(0)}(0)]^2\rangle = \frac{C}{5}\sum_i P_i^0 \frac{1}{r_i^6} \tag{A36}$$

which reduces to [35]

$$M_2^\infty = \frac{3}{2} C\langle F^{(0)}(t)\rangle^2 = \frac{1}{5} C \sum_{i,j} P_i^0 P_j^0 \frac{1}{r_i^3 r_j^3} P_2(\cos\Omega_{ij}) \tag{A37}$$

in the presence of motions fast enough to satisfy $\tau_c \ll (M_2^{rigid})^{-1/2}$. Here the dipolar coupled like-spin 1/2 system is considered for a simple example and in this case it holds that $C = \frac{9}{4}\gamma^4\hbar^2$. Eq. (A35) is the sum rule provided in Ref. [22],

$$M_2^{rigid} - M_2^\infty = \frac{1}{2\pi}\int_{-\infty}^{\infty} T_1^{-1}(\omega) d\omega, \tag{A38}$$

when the spin-lattice relaxation rate is expressed in the form of Eq. (A32). Therefore the property of the asymmetry of the potential wells can be obtained from the second moment of the NMR absorption line.

For the dipolar coupled unlike spins I and S, the longitudinal relaxation is described by a coupled differential equation pertaining to the respective magnetic species [21],

$$\begin{aligned}\frac{d}{dt}\Delta I_z &= -T_1^{-1}(\mathrm{II})\cdot\Delta I_z - T_1^{-1}(\mathrm{IS})\cdot\Delta S_z \\ \frac{d}{dt}\Delta S_z &= -T_1^{-1}(\mathrm{SI})\cdot\Delta I_z - T_1^{-1}(\mathrm{SS})\cdot\Delta S_z\end{aligned} \tag{A39}$$

where $\Delta I_z = \langle I_z\rangle - I_0$ and $\Delta S_z = \langle S_z\rangle - S_0$ are the deviations of the respective magnetizations from the equilibrium values. Using the power spectrum defined in Eqs. (A3) and (A4) the spin lattice relaxation rates are given by

$$\begin{aligned}T_1^{-1}(\mathrm{II}) &= \gamma_I^2\gamma_S^2\hbar^2 S(S+1)[J^{(0)}(\omega_I - \omega_S) + 3J^{(1)}(\omega_I) \\ &\quad + 6J^{(2)}(\omega_I + \omega_S)] \\ T_1^{-1}(\mathrm{IS}) &= \gamma_I^2\gamma_S^2\hbar^2 I(I+1)[-J^{(0)}(\omega_I - \omega_S) \\ &\quad + 6J^{(2)}(\omega_I + \omega_S)].\end{aligned} \tag{A40}$$

The expressions for $T_1^{-1}(\mathrm{SS})$ and $T_1^{-1}(\mathrm{SI})$ are obtained by interchanging the indices I and S of the above equations. In the case of powdered specimens, Eq. (A40) is given in the forms of

$$\begin{aligned}T_1^{-1}(\mathrm{II}) &= \gamma_I^2\gamma_S^2\hbar^2 S(S+1)\sum_l A_l B_{II}^{(1)}(\tau_{cl}) \\ T_1^{-1}(\mathrm{IS}) &= \gamma_I^2\gamma_S^2\hbar^2 I(I+1)\sum_l A_l B_{IS}^{(1)}(\tau_{cl})\end{aligned} \tag{A41}$$

where A_l is the geometry factor defined in Eq. (A30) and

$$\begin{aligned}B_{II}^{(1)}(\tau_c) &= j(\lambda_c, \omega_I - \omega_S) + 3j(\lambda_c, 2\omega_I) + 6j(\lambda_c, \omega_I + \omega_S) \\ B_{IS}^{(1)}(\tau_c) &= -j(\lambda_c, \omega_I - \omega_S) + 6j(\lambda_c, \omega_I + \omega_S).\end{aligned} \tag{A42}$$

The power spectrum $j(\lambda_c, \omega)$ is given in Eq. (A34).

The formulation described above is concerned with the relaxation due to the modulation of dipole coupling. Its generalization to other relaxation mechanism is straightforward. Spin relaxation rates are given by the superposition of the power spectra of the correlation functions appropriately defined for each relaxation mechanism [21]. The procedure of the calculation is exactly the same as described above and can be apply to the quadrupole coupling, anisotropic nuclear magnetic shielding (chemical shift anisotropy), and spin-rotation coupling. The details are given by Soda in his original manuscript [36].

A.2 A Simple Example of Two-Site Exchange Process in Unequal Potential Wells

The effects of asymmetry of the potential depths on the spin relaxation were pointed out in several reports [14, 15, 37, 38]. The formalism presented above is quite general and very useful for the formulation of spin relaxation for general multi-site exchange process in asymmetric potential wells. Let us consider at first the simple case that a single proton pair is jumping between the two orientations or sites with asymmetric double well potential such as the formulation of spin relaxation due to proton transfer in carboxylic acid dimers [13, 19]. In this case, the two potential minima are designated by I and II, where the minimum I is deeper and corresponds to the stable conformation. The first step of the derivation of spin relaxation formula is to construct the transition matrix $\boldsymbol{D}$ in Eq. (A14) and the equilibrium population vector $\boldsymbol{\xi}_0$ in Eqs. (A16) and (A18). Those are given by

$$\boldsymbol{D} = W_c\begin{pmatrix} 1 & -1 \\ -a & a\end{pmatrix} \tag{A43}$$

and

$$\boldsymbol{\xi}_0 = (P_I^0, P_{II}^0) = \frac{1}{1+a}(a, 1), \tag{A44}$$

where

$$a = \frac{W_{II\to I}}{W_{I\to II}} = \frac{P_I^0}{P_{II}^0} = e^{\Delta E/kT} \tag{A45}$$

is the population ratio of the two sites and $W_c = W_{I\to II}$ designates the inverse of the residence time at the site I which is more stable site. The transition matrix $\boldsymbol{D}$ can be transformed to symmetric matrix $\boldsymbol{d}$,

$$\boldsymbol{d} = \boldsymbol{V}^{-1}\boldsymbol{D}\boldsymbol{V}, \tag{A46}$$

where

$$\boldsymbol{V} = \begin{pmatrix} 1/\sqrt{P_{\mathrm{I}}^0} & 0 \\ 0 & 1/\sqrt{P_{\mathrm{II}}^0} \end{pmatrix} \tag{A47}$$

and matrix $\boldsymbol{d}$ may be diagonalized by the matrix $\boldsymbol{U}$,

$$\boldsymbol{U} = \begin{pmatrix} \sqrt{P_{\mathrm{I}}^0} & -\sqrt{P_{\mathrm{II}}^0} \\ \sqrt{P_{\mathrm{II}}^0} & \sqrt{P_{\mathrm{I}}^0} \end{pmatrix}. \tag{A48}$$

The matrix $\boldsymbol{d}$ has non-zero eigen value of

$$\Lambda = W_{\mathrm{I}\to\mathrm{II}} + W_{\mathrm{II}\to\mathrm{I}} = (1+a)\, W_{\mathrm{c}} = \tau_{\mathrm{c}}^{-1}. \tag{A49}$$

From Eqs. (A30) through (A34), the spin-lattice relaxation rate due to the motion between unequal potential wells is given by

$$T_1^{-1} = mCAB(\tau_{\mathrm{c}}) \tag{A50}$$

where

$$\begin{aligned} B(\tau_{\mathrm{c}}) &= \frac{\tau_{\mathrm{c}}}{1+\omega^2\tau_{\mathrm{c}}^2} + \frac{4\tau_{\mathrm{c}}}{1+4\omega^2\tau_{\mathrm{c}}^2} \\ A &= \frac{2}{15}\frac{a}{(1+a)^2}\{r_{\mathrm{I}}^{-6} + r_{\mathrm{II}}^{-6} + (1-3\cos^2\theta)\, r_{\mathrm{I}}^{-3} r_{\mathrm{II}}^{-3}\} \\ a &= \mathrm{e}^{\Delta E/RT} \\ \tau_{\mathrm{c}}^{-1} &= (1+a)\,\tau_{\mathrm{c}0}^{-1}\exp(-E_{\mathrm{a}}/kT). \end{aligned} \tag{A51}$$

The value r_{i} denotes the distance between the two protons in the i-th configuration and θ is the angle between the proton-proton vector of configurations I and II [19]. Arrhenius relation $\tau_{\mathrm{c}}^{-1} = \tau_{\mathrm{c}0}^{-1}\exp(-E_{\mathrm{a}}/kT)$ was assumed for τ_{c}^{-1}. In the case of phonon-assisted tunneling, τ_{c}^{-1} can be replaced by tunneling rate as Skinner and Trommsdorff proposed [13]. The value m in Eq. (A50) designates the fraction of protons directly relaxed among all of the protons present in the crystal, where we assume that the spin temperature is valid. For the case of r_{I}=r_{II}, the formulation of spin-lattice relaxation rate described by Eqs. (A50) and (A51) is exactly the same as that reported by Andrew and Latanowicz [37].

A.3 Formulation of T_1 of DNP for the Four-Site Exchange in Unequal Potential Wells

For DNP we consider the four-site exchange model schematically shown in Fig. 7. In this case direct exchange processes between II and IV and between I and III are neglected. Two transition rates (inverse of residence time) are represented by W_1 and W_2 for the transition from I to II (I to IV) and from II to III (IV to III), respectively. The transition rates were approximated by a sum of classical jump rate and the rate of phonon-assisted tunneling [13]. Fractional occupation at site i is given by P_{i}^0 (i=I, II, III, and IV) and it holds that

$$P_{\mathrm{I}}^0 + P_{\mathrm{II}}^0 + P_{\mathrm{III}}^0 + P_{\mathrm{IV}}^0 = 1. \tag{A52}$$

We assume that $P_{\mathrm{II}}^0 = P_{\mathrm{IV}}^0$ and then

$$\begin{aligned} P_{\mathrm{I}}^0 &= \frac{PQ}{Q(P+2)+1}, \\ P_{\mathrm{II}}^0 &= \frac{Q}{Q(P+2)+1}, \\ P_{\mathrm{III}}^0 &= \frac{1}{Q(P+2)+1}, \end{aligned} \tag{A53}$$

where

$$\begin{aligned} P &= \frac{P_{\mathrm{I}}^0}{P_{\mathrm{II}}^0} = \frac{P_{\mathrm{I}}^0}{P_{\mathrm{IV}}^0} = \exp(D_1/RT), \\ Q &= \frac{P_{\mathrm{II}}^0}{P_{\mathrm{III}}^0} = \frac{P_{\mathrm{IV}}^0}{P_{\mathrm{III}}^0} = \exp(D_2/RT), \\ PQ &= \frac{P_{\mathrm{I}}^0}{P_{\mathrm{III}}^0} = \exp((D_1+D_2)/RT). \end{aligned} \tag{A54}$$

The transition matrix $\boldsymbol{D}$ is given by

$$\boldsymbol{D} = \begin{pmatrix} 2W_1 & -W_1 & 0 & -W_1 \\ -PW_1 & PW_1+W_2 & -W_2 & 0 \\ 0 & -QW_2 & 2QW_2 & -QW_2 \\ -PW_1 & 0 & W_2 & PW_1+W_2 \end{pmatrix}, \tag{A55}$$

and it holds that $\boldsymbol{\xi}_0\boldsymbol{D} = \boldsymbol{0}$, where $\boldsymbol{\xi}_0 = (P_{\mathrm{I}}^0, P_{\mathrm{II}}^0, P_{\mathrm{III}}^0, P_{\mathrm{IV}}^0)$ as shown in Eq. (A16). The matrix $\boldsymbol{D}$ can be transformed to the symmetric one as described in Eq. (A21) and we obtain

$$\boldsymbol{d} = \begin{pmatrix} 2W_1 & -W_1\sqrt{P} & 0 & -W_1\sqrt{P} \\ -W_1\sqrt{P} & W_1P+W_2 & -W_2\sqrt{Q} & 0 \\ 0 & -W_2\sqrt{Q} & 2W_2Q & -W_2\sqrt{Q} \\ -W_1\sqrt{P} & 0 & -W_2\sqrt{Q} & W_1P+W \end{pmatrix}, \tag{A56}$$

which can be diagonalized by a unitary transformation $\boldsymbol{U}$,

$$\boldsymbol{U} = \begin{pmatrix} \sqrt{\frac{PQ}{PQ+2Q+1}} & 0 & \frac{2W_1\sqrt{P}(u-2QW_2)}{A} & \frac{2W_1\sqrt{P}(v-2QW_2)}{B} \\ \sqrt{\frac{Q}{PQ+2Q+1}} & \sqrt{\frac{1}{2}} & -\frac{(PW_1+W_2)u-2W_1W_2(PQ+1)}{A} & -\frac{(PW_1+W_2)v-2W_1W_2(PQ+1)}{B} \\ \sqrt{\frac{1}{PQ+2Q+1}} & 0 & \frac{2W_2\sqrt{Q}(u-2W_1)}{A} & \frac{2W_2\sqrt{Q}(v-2W_1)}{B} \\ \sqrt{\frac{Q}{PQ+2Q+1}} & \sqrt{\frac{1}{2}} & -\frac{(PW_1+W_2)u-2W_1W_2(PQ+1)}{A} & -\frac{(PW_1+W_2)v-2W_1W_2(PQ+1)}{B} \end{pmatrix} \tag{A57}$$

where

$$\begin{aligned} u &= \frac{\{(P+2)W_1 + (2Q+1)W_2\} + S}{2}, \\ v &= \frac{\{(P+2)W_1 + (2Q+1)W_2\} - S}{2}, \\ S &= \sqrt{\{(P+2)W_1 + (2Q+1)W_2\}^2 - 8W_1W_2(PQ+2Q+1)}, \\ A &= \sqrt{(u-2W_1)^2\{(u-2QW_2)^2 + 4W_2^2Q\} + \{(u-2W_1)^2 + 4PW_1^2\}(u-2QW_2)^2}, \\ B &= \sqrt{(v-2W_1)^2\{(v-2QW_2)^2 + 4W_2^2Q\} + \{(v-2W_1)^2 + 4PW_1^2\}(v-2QW_2)^2}. \end{aligned} \tag{A58}$$

Then a set of eigen values Λ_{i} is obtained,

$$\begin{aligned} \Lambda_1 &= 0, \\ \Lambda_2 &= PW_1 + W_2, \\ \Lambda_3 &= \frac{1}{2}\{(P+2)W_1 + (2Q+1)W_2 + S\}, \\ \Lambda_4 &= \frac{1}{2}\{(P+2)W_1 + (2Q+1)W_2 - S\}, \end{aligned} \tag{A59}$$

and non-zero eigen values correspond to the inverse of the correlation times,

$$\tau_1^{-1} = \Lambda_2 = PW_1 + W_2\,,$$
$$\tau_2^{-1} = \Lambda_3 = \frac{1}{2}\{(P+2)\,W_1 + (2Q+1)\,W_2 + S\}\,,$$
$$\tau_3^{-1} = \Lambda_4 = \frac{1}{2}\{(P+2)\,W_1 + (2Q+1)\,W_2 - S\}\,. \qquad \text{(A60)}$$

The coefficient A_l in Eq. (A30) can be exactly calculated by using U_{ij}, P_i^0, and the geometry of the DNP molecule determined by X-ray diffraction experiment. The analytical expression of T_1^{-1} (II) represented by Eq. (6) in Sect. (4.2) and by Eq. (A41) in this section is complicated and the coefficients A_l were calculated numerically from Eq. (A30).

References

[1] (a) M.D. Cohen and G.M.J. Schmit, J. Phys. Chem. *66*, 2442 (1962).
(b) M.D. Cohen, G.M.J. Schmit and S. Flavian, J. Chem. Soc. 2041 (1964).

[2] (a) E. Hadjoudis, I. Moustakli-Mavridis, F. Milia, J. Seliger, R. Blinc, and V. Zegar, Bull. Magn. Reson. *6*, 116 (1984).
(b) N. Hoshino, T. Inabe, T. Mitani, and Y. Maruyama, Bull. Chem. Soc. Jpn. *61*, 4207 (1988).

[3] (a) H. Rumpel and H.H. Limbach, J. Am. Chem. Soc. *111*, 5429 (1989).
(b) G. Scherer and H.H. Limbach, J. Am. Chem. Soc. *116*, 1230 (1994).
(c) J. Braun, H.H. Limbach, P.G. Williams, H. Morimoto, and D.E. Wemmer, J. Am. Chem. Soc. *118*, 7231 (1996) and references cited therein.

[4] (a) H.H. Limbach, B. Wehrle, H. Zimmermann, R. Kendrick, and C.S. Yannoni, J. Am. Chem. Soc. *109*, 929 (1987).
(b) B. Wehrle, H. Zimmermann, and H.H. Limbach, J. Am. Chem. Soc. *110*, 7014 (1988).
(c) B. Wehrle, F. Aguilar-Parrilla, and H.H. Limbach, J. Magn. Reson. *87*, 584 (1990).

[5] C.G. Hoelger, B. Wehrle, H. Benedict, and H.H. Limbach, J. Phys. Chem. *98*, 843 (1994).

[6] T. Inabe, I. Luneau, T. Mitani, Y. Maruyama, and S. Takeda, Bull. Chem. Soc. Jpn. *67*, 612 (1994).

[7] E. Ito, H. Oji, T. Araki, K. Oichi, H. Ishii, Y. Ouchi, T. Ohta, N. Kosugi, Y. Maruyama, T. Naito, T. Inabe, and K. Seki, J. Am. Chem. Soc. *119*, 6336 (1997).

[8] C. Benedict, U. Langer, H.H. Limbach, H. Ogata, and S. Takeda, Ber. Bunsenges. Phys. Chem. *102*, 335 (1998).

[9] S. Hayashi and K. Hayamizu, Bull. Chem. Soc. Jpn. *64*, 688 (1991).

[10] M. Witanowski, L. Stefaniak, and G.A. Webb, Annual Reports on NMR Spectroscopy 11 B, Academic Press, New York, 1981.

[11] G. Martin, M.L. Martin, and J.P. Gouesnard, NMR Basic Principles and Progress, Vol. 18, ^{15}N NMR Spectroscopy, Springer, Heidelberg, 1989.

[12] B.C. Chen, W. von Philipsborn, and K. Nagarajan, Helv. Chim. Acta, *66*, 153 (1983).

[13] J.L. Skinner and H.P. Trommsdorff, J. Chem. Phys. *89*, 897 (1988).

[14] D.C. Look and I.J. Lowe, J. Chem. Phys. *44*, 3437 (1966).

[15] M. Polak and D.C. Ailion, J. Magn. Reson. 26, 17 (1977); J. Chem. Phys. *67*, 3029 (1977).

[16] G. Soda, Kagaku no Ryoiki (J. Jpn. Chem.) *28*, 799 (1974).

[17] T. Yamamoto, Thesis, Osaka university, Japan, 1980.

[18] S. Takeda, G. Soda, and H. Chihara, Mol. Phys. *47*, 501 (1982).

[19] N. Imaoka, S. Takeda, and H. Chihara, Bull. Chem. Soc. Jpn. *61*, 1865 (1988).

[20] S. Takeda, K. Miyakubo, and H. Chihara, in: Studies in physical and theoretical chemistry, Vol. 67. Magnetic resonance and related phenomena, p. 791, eds. by J. Stankowski, N. Pislewski, S.K. Hoffmann, and S. Idziak, Elsevier, Amsterdam, 1989.

[21] A. Abragam, Principles of nuclear magnetism, Oxford Univ. Press, Oxford, ch. 8, 1961.

[22] G. Soda and H. Chihara, J. Phys. Soc. Jpn. *36*, 954 (1974).

[23] S. Takeda, H. Chihara, T. Inabe, T. Mitani, and Y. Maruyama, Chem. Phys. Lett. *189*, 13 (1992).

[24] A.J. Horsewill and A. Aibout, J. Phys. Condens. Matter, *1*, 9609 (1989).

[25] A. Stöckli, B.H. Meier, R. Kreis, R. Meyer, and R.R. Ernst, J. Chem. Phys. *93*, 1502 (1990).

[26] A.J. Horsewill, A. Heideman, and S. Hayashi, Z. Phys. B. *90*, 319, (1993).

[27] R.L. Hilt and R.S. Hubbard, Phys. Rev. A. *134*, 329 (1964).

[28] L.K. Runnels, Phys. Rev. A *134*, 28 (1964).

[29] S. Emid, R.J. Baarda, J. Smidt, and R.A. Wind, Physica B, *93*, 327 (1978).

[30] J. Tang, A. Pines, and S. Emid, J. Chem. Phys. *73*, 172 (1980).

[31] R. Kubo and K. Tomita, J. Phys. Soc. Jpn. *9*, 888 (1954).

[32] J. Haupt, Z. Naturforsch. A, *26*, 1578 (1971).

[33] W. Müller-Warmth, R. Shüler, M. Prager, and A. Kollmar, J. Chem. Phys. *69*, 2382 (1978).

[34] J.H. Van Vleck, Phys. Rev. *74*, 1168 (1948).

[35] H.S. Gtowsky and G.E. Pake, J. Chem. Phys. *18*, 162 (1950).

[36] G. Soda and H. Chihara, unpublished work.

[37] E.R. Andrew and L. Latanowicz, J. Magn. Reson. *68*, 232 (1986).

[38] L. Latanowicz and E.C. Reynmardt, Mol. Phys. *90*, 107 (1997).

Presented at the Discussion Meeting of the Deutsche Bunsen-Gesellschaft für Physikalische Chemie "Hydrogen Transfer: Experiment and Theory" in Berlin, September 10th to 13th, 1997 E 9991